AADE-12-FTCE-35

Cement Failure and Potential Wellbore Leakage Induced by Injection Loads

Runar Nygaard, Saeed Salehi, and Benjamin Weideman, Missouri University of Science and Technology

Abstract

Well integrity is one of the critical concerns when injecting CO_2 for EOR projects or carbon sequestration. Thermal stresses created while injecting cold CO_2 together with other mechanical loads can change the near wellbore hoop and radial stresses. These stress changes can cause de-bonding between casing-cement-formation and also create potential leakage path through initiating shear and tensile failures in the cement or formation.

The objective of this study was to conduct 3D finite element analysis to detect potential wellbore leakage paths in injection wells. This study based its well design data from existing wells in the Wabamun area in Alberta (Canada). The integrity of existing wells in this area was recently investigated as part of a CO_2 sequestration feasibility study led by University of Calgary.

Cement material properties were determined with rock mechanical testing including Young's modulus, Poisson's ratio, tensile strength and unconfined compressive strength. Thermal extension, heat capacity and thermal conductivity were measured on cement mold samples.

Multi-stage simulations for casing-cement and cement-formation interactions with temperature enabled elements were conducted. Simulation results indicate that thermal cooling effect near-wellbore stresses will increase risk of integrity loss in casing-cement and cement-formation. Risk of de-bonding and tensile failure will increase with increasing cement Young's modulus and Poisson's ratio under dynamic loading conditions. In addition, having very low mechanical strength will increase the risk of shear failure in the cement.

Introduction

Wellbore leakage is an identified as a problem for injection wells [1-3]. An important part of a successful injection project is to avoid any leakage along the wellbore with a well executed cement placement in the wellbore annulus. Even with a good primary cement sheet initially the cement integrity might change over the life of the well. One area of active investigation is the fate of cement in CO_2 injection wells caused by chemical instability of Portland cement when it is reacting with CO_2 [4,5]. The Portland cement will react with the CO_2 and increase cement porosity when large volumes of CO_2 are present and with the right temperatures over time [6,7] Another long term effect of CO_2 injection is that the injection can impose several stresses on well casing, casing and cement boundaries and formation. Change in thermal stresses caused by cooling or heating may damage the integrity of the wellbore and most likely to the cement integrity. Cement failure will create new leakage path ways for gas to flow. In addition, it is costly to perform work-over operations to squeeze new cements or replace failed casings.

The wellbore can mechanically fail in different modes. Tensile stresses at the casing-cement interface and the cement-rock interface will likely cause de-bonding and opening of fluid pathways at the interface. Tensile stresses inside the cement or the rock can cause tensile fracturing if the stresses reach the tensile strength of the material. The tensile strength of steel is so high that that tensile failure is not likely to occur in the casing. Shear stresses inside the cement or the rock can cause shear fractures to form which also can destroy the integrity of the wellbore and act as leakage pathways.

This paper aims to study integrity of casing, cement, and rock and also the casing-cement interface and the cement-rock interface during CO_2 injection. The cold injection fluid can cause both reductions in wellbore temperature as well as higher fluid pressures on the wellbore. Both laboratory experiments and numerical models are conducted. A finite element model of a cased well in the injection area was built to investigate the effect of thermal and pressure loading on well integrity.

Alberta field study description

Large stationary CO_2 emitters are located in central Alberta with cumulative annual emissions in the order of 30 Mt CO_2. This includes four coal-fired power plants in the Wabamun Lake area, southwest of Edmonton with emissions between 3 to 6 Mt per year. To sequester the emitted CO_2 locally the Wabamun Lake area southwest of Edmonton was identified as a potential site for future large-scale CO_2 injection [8]. University of Calgary led a comprehensive feasibility study of large-scale CO_2 storage opportunities in central Alberta named the Wabamun Area CO_2 Sequestration project (WASP) [9].

As part of the WASP study well integrity and wellbore leakage was investigated. Of the 1000 wells in the study area only 95 wells penetrated the immediate Calmar shale which was the cap rock sealing the proposed Nisku carbonate injection formation. The 95 wells were identified as potential leakage pathways. The leakage risk of these wells was evaluated based on the knowledge of well design, current well status and historical regulation's in the area. For the subset of

27 well studied on only 4 wells were identified as wells requiring work over which was less of a problem than anticipated [10]. For a typical cased wellbore in the area a (229 mm) production hole is drilled and a 7 in (177.8 mm) J-55 20 lb/ft (6.456 in ID) production casing. This gives a cement sheath thickness of 2 inch. The production cement is made up of standard Portland cement with 2 % CaCl and sometimes a small percentage of bentonite (gel) [10].

Model Development and Simulation Approach

The goal for this study was to conduct a three-dimensional finite-element model using elasto-plastic material models for the cement sheath in a cased annulus and the formation. A multi-stage simulation for casing-cement and cement-formation interactions with temperature enabled elements was conducted [11].

Most of the previous numerical approaches emphasized on studying cement integrity when cement has been set and the mechanical and/or thermal loadings were applied to the model [12-17]. The procedure here is different in terms of building the loading histories through multi-stage non-linear finite-element analysis. The advantage of building the model in several steps is to observe and record stress and deformation changes after each loading, furthermore knowing previous deformation and loading history will help to specify initial stress state before final thermal and mechanical loads applied to the model [18].

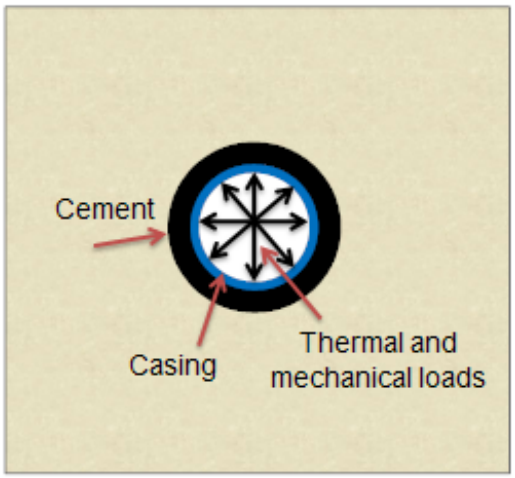

Figure 1. Thermal and mechanical loads were applied on the near wellbore model (7 in J-55 20 lb/feet casing, 2 in neat cement and a 9 in wellbore in the Nisku shale formation) [11]

Figure 1 shows a schematic of the borehole cross section and the loads (mechanical and thermal) that are applied on them. Details of the steps followed in numerical simulations can be described as follow:

Step 1. Loading the model with in-situ stress: In this step two horizontal stresses (minimum and maximum) and overburden stress are applied to the all elements in the model (43.7 MPa, 41.8 MPa and 38 MPa for overburden, maximum and minimum horizontal stresses respectively). An initial temperature of 60°C for reservoir temperature was applied to all the nodes. Table 1 summarizes rock mechanical properties used for different materials in the model. Elasto-plastic material model is used for formation elements to observe yielding history through different loading steps.

Step 2. Drilling step: In this step wellbore elements removed from the model, and mud pressure applied to the wellbore face. Stress equilibration was achieved at the end of the step and near wellbore stresses was imposed. This step simulates drilling process of the borehole.

Step 3. Running Casing: Casing elements were introduced to the model at this step with mud pressure applied to the inside and outside of the casing. Linear-elastic behavior was assumed for the casing elements.

Step 4. Cementing: At this stage cement elements were introduced to the model. The cement elements were fully bonded to the formation. These elements were also activated by zero deformation but under initial hydrostatic slurry pressure because the cement is not yet hardened it will equal hydrostatic pressure. This status is defined as initial conditions for the cement elements before loading step starts. Mohr-Coulomb softening material model is applied for cement elements, which is essential for predicting plastic failure in cement when thermal and mechanical loads are applied to the model.

Step 5. Applying thermal and mechanical loads: After cement and casing were set, the final stage is to apply thermal and mechanical loads for the cased wellbore. Mechanical loads were applied by using distributed load on casing surface and thermal load was defined by putting thermal boundary conditions on casing nodes. One day's worth of temperature change using a transient model was simulated to allow the boundaries to remain at their initial temperature. The elements used for casing, cement and formation have features for coupled thermal-displacement analysis with the options to define thermal conductivity, thermal expansion and specific heat values.

Laboratory Tests

Linear Thermal Expansion Coefficient

The linear thermal expansion coefficient (α) is defined as strain per change in temperature. The α value is required to describe the effect of a temperature changes in a material. When a material is constrained by other materials additional stresses can form as temperature changes. Equation 1 below describe α in obtained experimentally, with C as a correction factor.

$$\alpha = \frac{\Delta L - C \cdot \Delta T}{L \cdot \Delta T} \quad (1)$$

α is obtained by measuring deformation caused by temperature change of a submerged cylindrical cement sample. The apparatus consists of ¾ in steel frame, a temperature probe, a linear vertical deformation transducer (LVDT), a glass beaker filled with water. The water temperature is heated a constant temperature is reached in the water and the cement sample. Once temperature is stabilized the initial measurement is taken. As the sample and water cool the sample will shrink proportional to its thermal expansion coefficient and as this occurs the LVDT measures this change in length. The temperature versus displacement results are calibrated with a 316 stainless steel sample value and a linear regression determines the thermal expansion coefficient.

Sonic Velocity

The parameters determined from the sonic velocity tests are compressional (Vp) and shear wave (Vs) velocities. These values are then substituted into Equations 2, to 5 to find dynamic elastic deformation properties [19]. These are important mechanical properties that can be correlated to the static properties for quick determination of static properties without the use strain gages or other devices.

$$v = \frac{V_p^2 - 2V_s^2}{2\left(V_p^2 - V_s^2\right)} \tag{2}$$

$$E = \frac{\rho V_s^2 (3V_p^2 - 4V_s^2)}{V_p^2 - V_s^2} \tag{3}$$

$$K = \frac{\rho(3V_p^2 - 4V_s^2)}{3} \tag{4}$$

$$G = \rho V_s^2 \tag{5}$$

v is Poisson's ratio, E is Young's modulus, K, is bulk modulus and G is shear modulus respectively. The sonic velocity apparatus consists of the signal generator, the emitter and receiver sensors, and Ultrasonic software [20]. The P and S wave velocities are measured by measuring the transit time of each wave through the test sample. The sample is placed between the two sensors and the software will measure the transit time by measuring the first peak of the emitted wave. The samples were heated to different temperatures and transit times were measured to determine if there is a relationship between the dynamic mechanical properties and temperature.

Divided Bar Thermal Conductivity

To measure thermal conductivity divided bar apparatus tests were conducted. Thermal conductivity is dependent on the heat flow, sample length, and temperature change as describe in Equation 6.

$$k = \frac{q \cdot x}{\Delta T} \tag{6}$$

The divided bar apparatus consist of highly heat conductive material, a lower conductivity material with known conductivity, and the test sample (Figure 2).

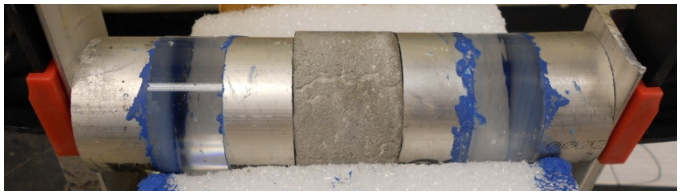

Figure 2. Divided bar experiment with cement cylinder. The length and diameter of the cement sample is two inch.

The apparatus in Figure 2 has a heat source which transfers heat up the aluminum to the first high conductivity aluminum and the cooler ambient room temperature is on the aluminum on the other side which transfers to the aluminum cylinder. The aluminum is attached to the known material by silicone adhesive which is chosen due to silicone's high conductivity. The test sample which is not permanently attached is kept in full contact with the aluminum by silicone grease, which was also chosen for silicone's high thermal conductivity. The thermal conductivity can only be found when the apparatus reaches steady-state. In order to get results in a more reasonable time frame thermal conductivity will be measured at every hour before steady-state and using a translated power regression the thermal conductivity can be projected to steady-state.

Calorimeter Specific Heat Capacity

Specific heat capacity [c], defined as the heat needed to raise a mass one degree temperature and is needed in time dependent models because as heat flows heat capacity will define the temperature of the material. It is given as;

$$[c] = \frac{\Delta Q}{\Delta T * m} \tag{7}$$

where ΔQ is heat flow, m is mass, and ΔT is temperature change. The specific heat capacity apparatus is a calorimeter which consists of a known mass of water and a known mass sample and known temperatures. The water is insulated so it operates as a closed system. The water temperature is recorded and then the sample of its own recorded temperature is placed into the water. The final water temperature is measured when it becomes constant.

Brazilian Tensile Test

The tensile strength of the cement was measured in a Brazilian tensile test apparatus. Rock and cements have relatively low tensile strengths compared to metals in the casing. The lower strength in the rock and the cement makes it a very likely failure mode which can form damaging fractures. Equation (8) gives the tensile strength in a Brazilian test set up.

$$T_o = \frac{2 \cdot P}{\pi \cdot D \cdot t} \quad (8)$$

where P is failure force, diameter D, and thickness t. The cement sample is cut into a 2 in diameter by 1 in thickness and placed between two curved pieces of steel. A hydraulic piston is lower as a loading rate of 50psi/min, and the force is recorded by the load sensor above the curved steel. The maximum force reading is used to determine the tensile strength.

Uniaxial Compression Test

To measure the unconfined compressive strength uniaxial compression tests were conducted on 2 inch diameter cement samples.

Laboratory Test Results

The laboratory results for a neat cement class H Portland cement are given in Table 1. These values combined with the casing and Calmar-shale properties from [21] were used for the finite-element simulations. The cohesion was calculated from the unconfined compressive strength and friction angle.

Table 1. Material properties used in the model

Material	Casing	Cement	Calmar-shale
E (GPa)	200	25	24.8
Poisson's ratio	0.3	0.2	0.27
C_0 (MPa)	-	45	-
Friction Angle (°)	-	30	35
Cohesion (MPa)	-	15	25.9
Thermal Expansion (10^6/K)	11.433	9.4	10
Thermal Conductivity (w/m-K)	43	0.25	0.27
Specific Heat (J/kg-K)	490	1020	900
Tensile Strength (MPa)	-	1.4	-

Finite-element simulations of cementing stages

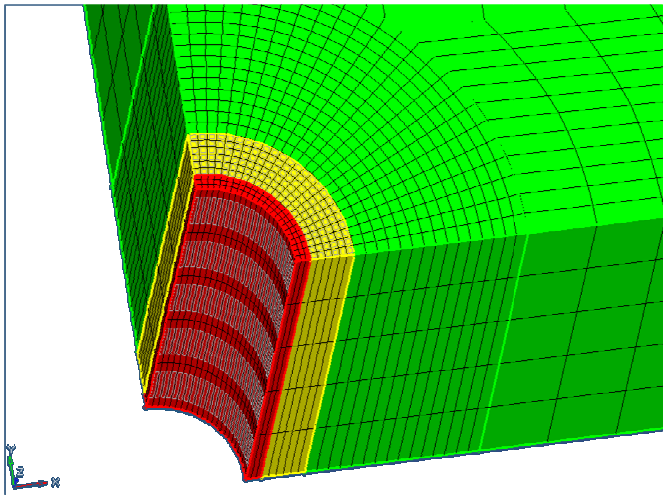

Figure 3. A Close-Up of the Three Dimensional Mesh built for Simulation.

The three-dimensional mesh has one and five meter length in z and (x,y) directions respectively (Figure 3). This allows minimizing end effects during simulations. Because of the symmetry conditions around the wellbore, only results for one-quarter is presented. The model in Figure 3 includes three materials with individual properties defined for each. The red elements above represent casing elements, the yellow elements represent cement elements, and the green elements represent formation elements. The grey on the inside of the casing elements are two dimensional surface elements that occur between the casing and cement and also between the cement and formation. The aspect ratio for the elements in the circular sections is <2.0 for the x-y plane providing more accurate estimations.

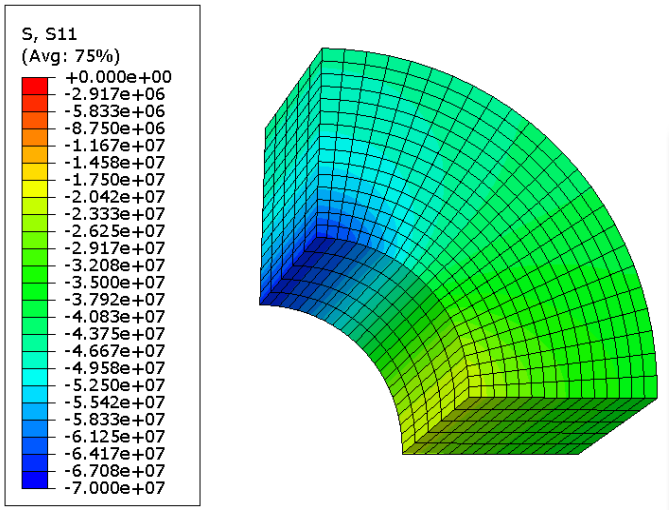

Figure 4. Stress distributions in the model, given in Pascal, after wellbore elements removed and mud weight applied (In Maximum Horizontal Stress Direction, X direction to the right)

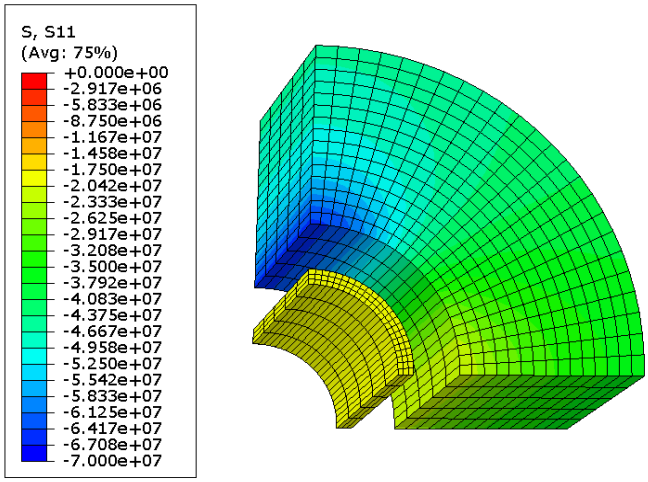

Figure 5. Stress distributions, in Pascal, after casing is added and mud weight is applied to the casing. (In Maximum Horizontal Stress Direction, X direction to the right)

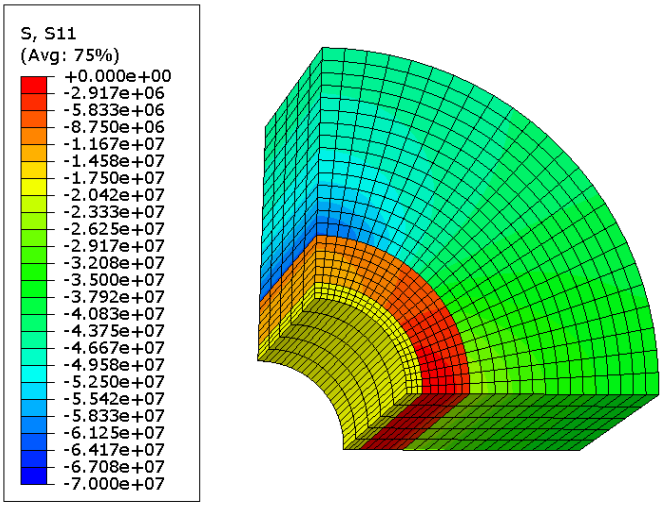

Figure 6. Stress distributions, in Pascal, after cement is added. (In Maximum Horizontal Stress Direction, X direction to the right)

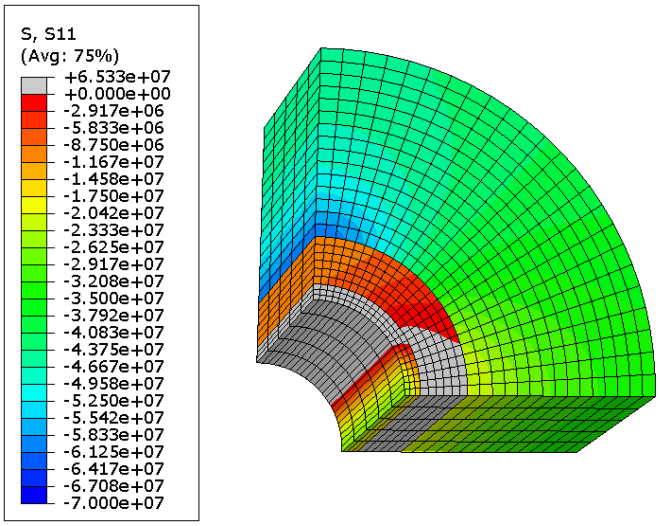

Figure 7. Stress distribution, in Pascal, after injection pressure of 27 MPa and 1 day of 20°C is applied to the inside of the casing. (In Maximum Horizontal Stress Direction, X direction to the right)

Figure 4 to 6 shows the stress distribution in the models at the different modeling steps before mechanical and thermal loading. Figure 4 corresponds to the second step of the model development when the bore hole is drilled and the wellbore is filled with mud. The stresses are negative which means that the formation is in compression and stable. Figure 5 correspond to step three when casing is run. The casing in the hole does not change the stresses at the wellbore wall since they are controlled by the mud pressure as expected. Figure 6 corresponds to step four when the cement is placed in the wellbore. The cement is replacing the mud and causes the stresses to change in the formation due to higher density of the cement than the drilling fluid. The simulation results in Figure 5 show that all stresses are compressive both in the casing, cement and formation and no sign of fracturing or de-bonding occurs. It should be noted that the model does not take into consideration any cement shrinkage.

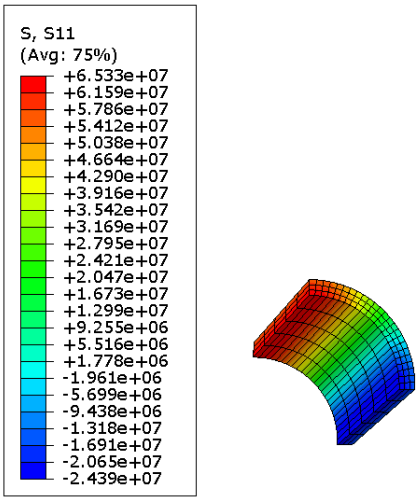

Figure 8. Stress distribution in the casing after injection pressure of 27 MPa and 1 day of 20°C is applied to the inside of the casing. (In Maximum Horizontal Stress Direction, X direction to the right)

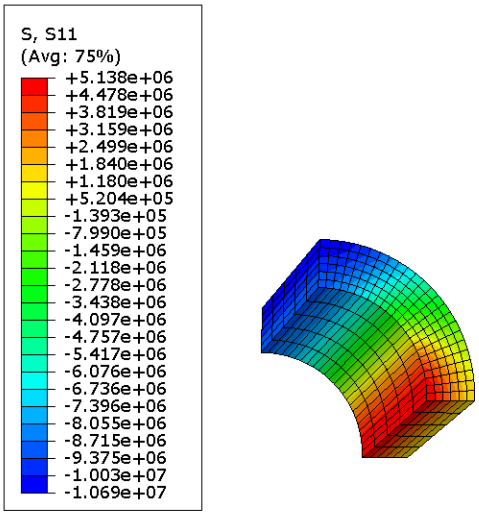

Figure 9. Stress distribution in the cement after injection pressure of 27 MPa and 1 day of 20°C is applied to the inside of the casing. (In Maximum Horizontal Stress Direction, X direction to the right)

Figure 7 shows the stress in the model at step 6 in the procedure which is after injection has caused pressure at the casing increasing with 7 MPa and the temperature at the

casing surface is cooled down 20 °C. The grey color in Figure 7 represents tensile stress zone in the model. Where there is tension there is the possibility of fractures forming depending on tensile strength of the material. Additionally, if tension occurs on the boundary between casing and cement or cement and rock there is the threat of de-bonding. The results show that in the maximum horizontal stress direction there is a potential of radial de-bonding.

The Calmar shale formation does not get in tension as seen in Figure 7 and would therefore will not form tensile fractures. Figure 8 and Figure 9 is a cut out of the results in Figure 7 for the casing and cement respectively. Using the values from the Brazilian tensile strength tests for the cement the risk for tensile failure begins typically at 1.4 MPa. The legend in Figure 8 displays that the yellow zone would be just below that risk and orange to red is above the tensile strength for cement and therefore tensile fractures forms.

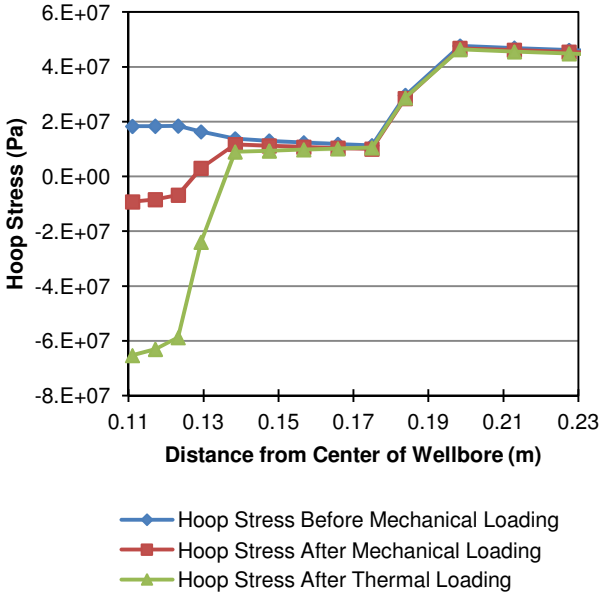

Figure 10. Hoop stress in maximum horizontal stress orientation before mechanical loading, after mechanical loading and after thermal loading.

Detailed presentation of the hoop and radial stresses in the maximum horizontal stress direction are provided in Figures 10 and 11, respectively. Figure 10 which shows the hoop stress results based on distance from the center of the cased borehole before any loading (blue line), after mechanical loading (red line) and after thermal loading (green line). Hoop stresses have dropped in all three materials after each loading. And more significantly, it has dropped into tension for the casing after thermal loadings because of the high thermal conductivity and linear thermal expansion coefficient of the casing and also because CO_2 injection pressure is applied at the casing surface. The results show that no radial fracture is created in the cement, however these results are only for one load cycle. The risk of tensile failure will be increased if more cycles be added through the well's life. There is no indication of any radial tensile fracture in the formation after thermal and mechanical loads. Figure 11 shows the radial stress results based on the distance from the center of the cased borehole before any loading (blue line), after mechanical loading (red line) and after thermal loading (green line). Radial stresses after mechanical loadings are decreased in the cement and formation and most significantly in the cement where the stresses become tensile. The tension in the cement at the boundary indicates the possibility of de-bonding at the casing and formation.

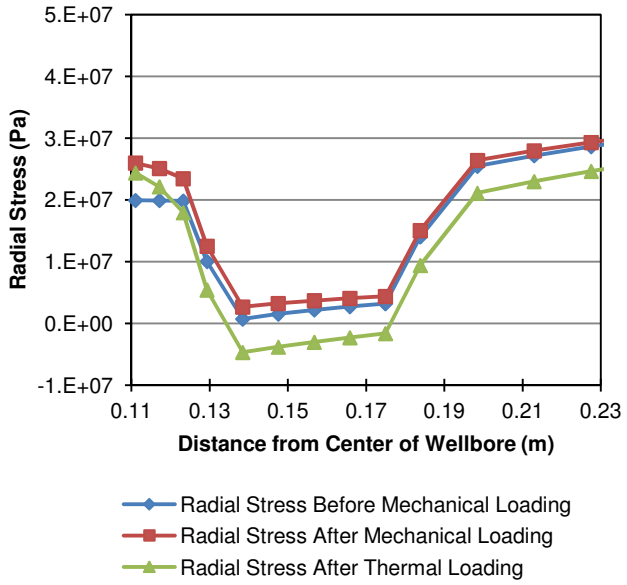

Figure 11. Radial stress in maximum horizontal stress orientation before mechanical loading, after mechanical loading and after thermal loading.

Parametric Study

Since the value of mechanical properties vary depending on the composition of the cement it was decided to run a parametric study on linear elastic properties of the cement to study cement sheath integrity under different loads when mechanical properties of the cement changes. Young's modulus (E) was reduced from base case (E=25 MPa) to E=5 MPa and increased to E=45 MPa. Figure 12 (Blue line for E=25, red line for E=5 and green line for E=45) shows hoop stress, in the maximum horizontal stress orientation, results for the cased wellbore with changing cement stiffness. For higher Young's modulus, tension was not induced into the cement. This indicates that increasing cement Young's modulus will not risk cement failure. Figure 13 shows radial stress in maximum horizontal stress orientation for the cased wellbore. As Young's modulus decreases de-bonding can be prevented.

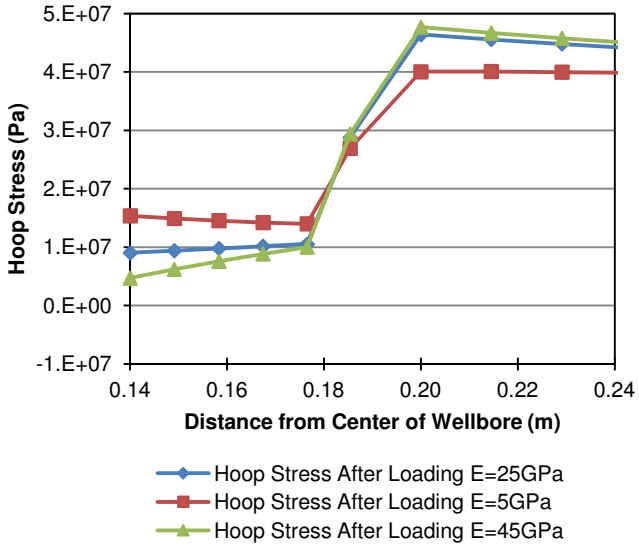

Figure 12. Hoop stress in maximum horizontal stress orientation (cement and formation) for E=25 MPa (Base Case), E=5 MPa and E=45 MPa.

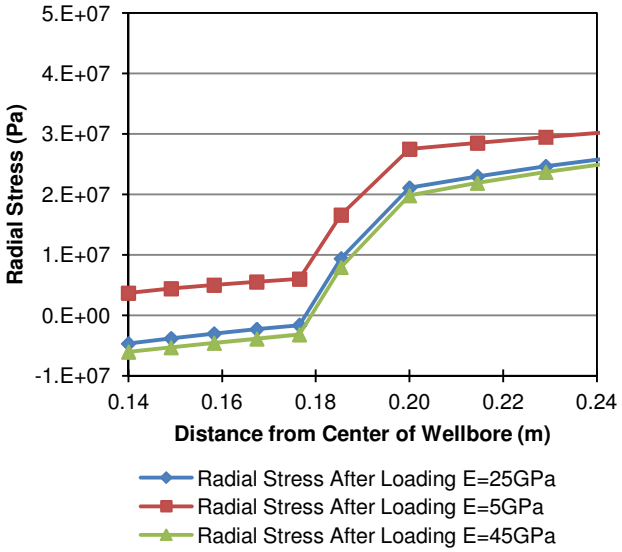

Figure 13. Radial stress in maximum horizontal stress orientation (cement and formation) for E=25 MPa (Base Case), E=5 MPa andvE=45 MPa.

In the next run of simulations, the Young's modulus (E=25 MPa) was fixed and Poisson's ratio was first reduced to 0.05 and then increased to 0.4. Figure 14 shows the hoop stress in maximum horizontal stress orientation for cement and formation in three cases (Blue line for base case, Poisson's ratio=0.2, red line for Poisson's ratio=0.05 and green line for Poisson's ratio=0.4). Figure 15 shows radial stress results for cement and formation for the three cases. The results indicate that when the Poisson's ratio reaches 0.4 radial de-bonding in casing-cement boundary will occur. The results also show that as the Poisson's ratio decreases to 0.05 de-bonding remains at the casing/cement boundary but the possibility of de-bonding at the cement/formation boundary decreases.

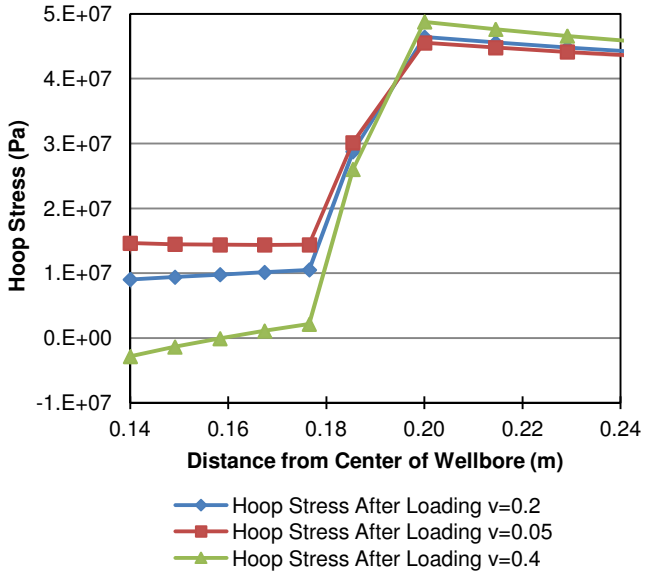

Figure 14. Hoop stress in maximum horizontal stress orientation (cement and formation) for Poisson's ratio=0.2 (Base Case), Poisson's ratio=0.05 and Poisson's ratio=0.4.

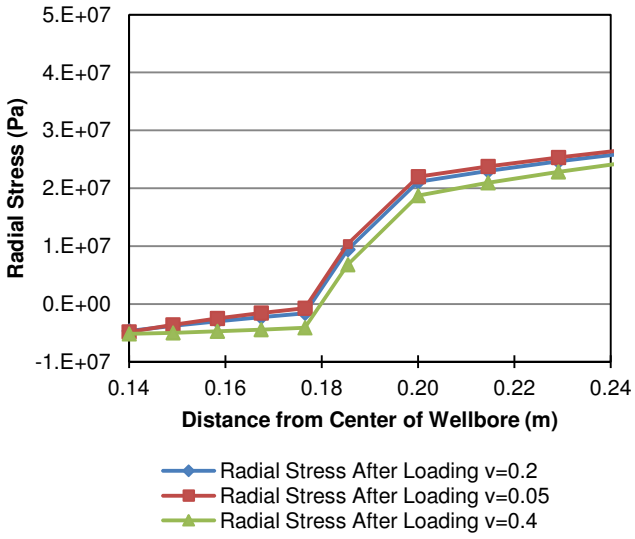

Figure 15. Radial stress in maximum horizontal stress orientation (cement and formation) for Poisson's ratio=0.2 (Base Case), Poisson's ratio=0.05 and Poisson's ratio=0.4.

Overall, the results indicate that cements with lower Young's modulus and Poisson's ratio will perform better under dynamic loading conditions. However, shear failure of the cement while loading can be very detrimental to cement integrity especially if the cement does not have enough strength. Figure 16 shows plastic strain results for cement with 5 MPa Young's modulus and 0.05 Poisson's ratio. The results indicate shear

failure in the cement elements when loadings applied to the model. This indicates the importance of a balance between cement mechanical properties and adjacent formation and casing properties for dynamic loading conditions.

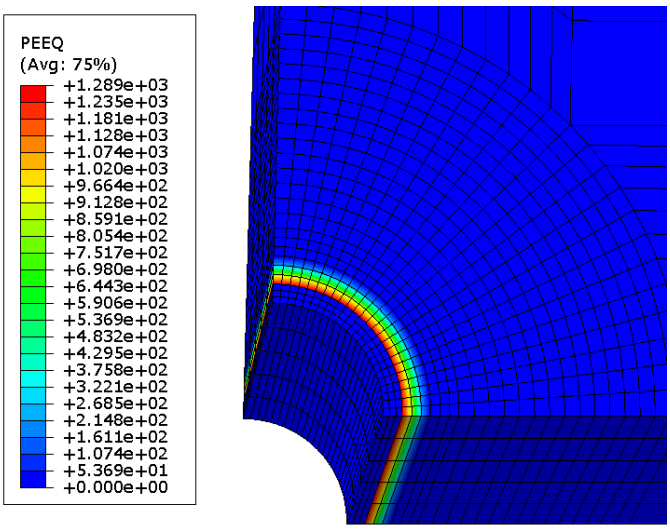

Figure 16. Plastic strains (shear failure) created in cement elements while loading.

Discussion

The variations in cement mechanical properties required a parametric study to evaluate the influence of different properties such as Young's modulus and Poisson's ratio. Increasing the Young's modulus will not induce radial fractures, but will increase the amount of de-bonding that might occur between the casing/cement and cement/formation boundaries. Decreasing Young's modulus will reduce de-bonding to none if the value is around 5 GPa, the issue would be the reduced strength associated with a lower Young's modulus. Increasing the Poisson's ratio to around 0.4 radial fractures occurred near the casing which was not present for the base case of Poisson's ratio of 0.2. Decreasing the Poisson's ratio will reduce the probability of de-bonding at the cement/formation boundary, but will keep the de-bonding at the casing/cement boundary and circumferential fractures from occurring.

Conclusions

This paper discussed the effects of mechanical and thermal loads caused by injection on cased wellbore integrity. This was done using experimentally derived cement properties and finite-element simulations on a typical cased well design in the Wabamun area in Alberta, Canada.

The results of the simulations showed that the mechanical load of injection did not result in wellbore failure or cement de-bonding but the temperature load did result in cement tensile failure (circumferentially) and de-bonding. Reducing Young's modulus reduces the potential for tensile failure and de-bonding can be prevented. Increased Poisson's ratio can cause radial fractures to happen.

Low Young's modulus and low Poisson's ratio are the best for preventing tensile failure and de-bonding, but the reduced cement strength can cause shear failure and plastic yielding. This shows the importance of balancing cement mechanical properties and wellbore stresses for any given situation.

Nomenclature

A= *Area of Sample, m^2*
α = *Linear Thermal Expansion Coefficient, $\mu\varepsilon/℃$*
C= *Measured Compressive Strength, lb*
C_o= *Unconfined Compressive Strength, MPa*
[c]= Specific Heat Capacity, J/kg-K
D= *Diameter of Sample, mm*
E= *Young's modulus, MPa*
ε = *Strain, m/m*
F= *Force on Sample, lb*
G= *Shear or Rigidity Modulus, MPa*
K= *Bulk Modulus, MPa*
L = *Length, mm*
q= *heat flow rate, W*
m= *Mass, kg*
μ = *Micro, 10^{-6}*
v= *Poisson's ratio*
P= *Brazilian Load Strength, lb*
Q= *Heat, J*
ρ= *Density, kg/m^3*
σ= *Stress, MPa*
t= *Thickness of Sample, mm*
T = *Temperature, Kelvin*
T_o= *Tensile Strength, MPa*
V_p= *P-Wave or Compressional Wave Velocity, m/s*
V_s =*S-Wave or Shear Wave Velocity, m/s*
x= *Length, m*

References

1. Randhol, P., and Carlsen, I.M,. 2008. Assessment of Sustained Well Integrity on the Norwegian Continental shelf. 4th meeting of the IEA-GHG Wellbore Integrity Network, 18th- 19th March, 2008 Paris France.
2. NPA, 2008. Norwegian Petroleum Safety Authority, 2008. Well integrity survey phase 1. www.ptil.no.
3. Watson, T.L., and Bachu, S., 2007. Evaluation of the Potential for Gas and CO2 Leakage along Wellbores. SPE 106817. E&P Environmental and Safety Conference, 5-7 March 2007, Galveston, Texas, U.S.A.
4. Shen, J., and Pye. D., 1989, Effects of CO2 attacks on Cement in High Temperature Applications, SPE/IADC 18618, presented at SPE/IADC drilling conference, New Orleans, LA, February 28- March 3, 1989.
5. Bachu, S., and Bennion, B., 2008. Experimental assessment of brine and/or CO2 leakage through well cements at reservoir conditions, International Journal of Greenhouse Gas Control. Volume 3, Issue 4, July 2009, Pages 494-501.
6. Kutchko B. G., Strazisar B. R., Dzombak D.A., Lowry G.V., and Thaulow N., 2007. Degradation of wellbore cement by CO2 under geologic sequestration conditions, Environ Sci. Technol. 41, p 4787-4792.
7. Barlet-Gouédard V., Rimmelé G., Goffe, B., and Porcherie, O., 2006. Mitigation strategies for the risk of CO2

migration through wellbores. SPE paper 98924. Proceedings of the 2006 IADC/SPE Drilling Conference, Miami Florida, 21-23 February 2006.

8. Michael, K., Bachu, S., Buschkuehle, M., Haug, K., Grobe, M., and A.T. Lytviak. 2006. Comprehensive Characterization of a Potential Site for CO2 Geological Storage in Central Alberta, Canada, CO2SC Symposium, Lawrence Berkeley Laboratory, Berkeley, California, March 20-22, 2006, 134-138.
9. Lavoie, R. and Keith, D., 2010, Wabamun area CO2 sequestration project (WASP) Final report. http://www.ucalgary.ca/wasp/Executive%20Summary.pdf
10. Nygaard, R., and Lavoie, R., 2010. Well Integrity and Workover Candidates for Existing Wells in the Wabamun Area CO2 Sequestration Project (WASP). SPE Paper 137007, presented at Canadian Unconventional Resources and International Petroleum Conference, 19-21 October 2010, Calgary, Alberta, Canada.
11. Nygaard, R., Salehi, S., and Lavoie, R. 2011. Effect of Dynamic Loading on Wellbore Leakage for the Wabamun Area CO2 Sequestration Project, SPE Annual Technical Conference and Exhibition, Canadian Unconventional Resources Conference (11CURC), 15 - 17 Nov 2011, 2011.
12. Jo, H., and Gray, K.E. 2010. Mechanical behavior of concentric casing, cement, and formation using analytical and numerical methods. 44th US Rock Mechanics Symposium, Salt Lake city, UT, June 27-30, 2010.
13. Ferla, A., Lavrov, A., and Fjaer, E. 2009. Finite element analysis of thermal-induced stresses around a cased injection well, 7th International Conference on Modern Practice in Stress and Vibration Analysis. Journal of Physics,181.
14. Shahri, M.A., Schubert, J.J., and Amani, M. 2005. Detecting and Modeling Cement Failure in High-Pressure/High-Temperature (HP/HT) Wells Using Finite Element Method (FEM). Paper IPTC 10961 presented at the International Petroleum Technology Conference, Doha, 21-23 November.
15. Rodriguez, W.J., Fleckenstein, W.W., and Eustes, A.W. 2003. Simulation of Collapse Loads on Cemented Casing Using Finite Element Analysis. SPE Paper 84566 presented at the SPE Annual Technical Conference and Exhibition, Denver, 5-8 October.
16. Heathman, J., and Beck., F.E. 2006. Finite Element Analysis Couples Casing and Cement Designs for HP/HT Wells in East Texas. SPE Paper presented at IADC/SPE Drilling conference, Miami, FL, 21-26 February.
17. Fleckenstein, W.W., Eustes, A.W., and Miller, M.G. 2000. Burst Induced Stresses in Cemented Wellbores. SPE Paper 62596 presented at SPE/AAPG Western Regional Meeting, California, 19-23 June.
18. Gray, K., Podnos, E., and Becker E., 2007. Finite Element Studies of Near-Wellbore Region During Cementing Operations: Part I. Production and Operations Symposium, 31 March-3 April 2007, Oklahoma City, Oklahoma, U.S.A. SPE-106998.
19. Barton, N., 2007. Rock Quality, Seismic Velocity, Attenuation and Anisotropy, Balkema-Proceedings and Monographs in Engineering, Water and Earth Sciences, Taylor & Francis, London, p729.
20. GCTS, 2004. Ultrasonics User's Guide and Reference. Geotechnical Consulting & Testing System. 2004. Unpublished user guide.
21. Nygaard, R., 2010. Geomechanical Analysis: Wabamun Area CO2 Sequestration Project (WASP), 2010. Energy and Environmental Systems Group. http://www.ucalgary.ca/wasp/Geomechanical%20Analysis.pdf